Fractional Power Damping Model of Joint Motion

James C. Houk[1] Andrew H. Fagg[2]
Andrew G. Barto[2]

houk@casbah.acns.nwu.edu
[1]Department of Physiology
Northwestern University School of Medicine
Chicago, IL 60611-3008

{fagg, barto}@cs.umass.edu
[2]Department of Computer Science
University of Massachusetts
Amherst, MA 01003-4610

November 9, 2000

Abstract

The control of arm movement involves an intricate interplay between descending commands, musculoskeletal mechanics and spinal reflexes. Computational studies focusing on brain mechanisms for generating movement commands would profit from the availability of a neuromuscular model that captures key complexities of the biological system while preserving an abstract framework to facilitate simulation. One important component of the model is the fractional power damping (FPD) that is produced by the stretch reflex. In this chapter, we describe a model that unites FPD and other prominent reflex features with a Hill-based lumped parameter model of the elbow musculature. In this FPD model, antagonist muscle bursts that function to decelerate the ongoing movement are generated by the stretch reflex, with central commands preserving some influence over the precise timing and magnitude of this response. Although descending control is achieved by setting equilibrium points of the viscoelastic muscle-reflex system, the nonlinear damping behavior of opposing reflexes interacts to

produce a region of stiction around the specified equilibrium. This slows movement so dramatically that the equilibrium point is effectively never reached in most movements. The complexities of these nonlinearities do not necessarily increase the difficulty of the central control problem. Effective control can be achieved by precisely timing the offset of the agonist burst, and the tendency for oscillations around the endpoint is greatly diminished by the stiction that results from fractional power damping.

1 Introduction

No one doubts that the spinal cord plays an important role in movement control. However, when it comes to deciding how motor functions are divided between the brain, the spinal cord and the musculoskeletal system, one elicits a wide range of opinion. This range of opinion is partly due to the variety of movements that may be considered. For example, basic aspects of locomotion and scratching are built into the spinal circuitry and require the least guidance from supraspinal networks. Voluntary reaching, grasping and manipulation of objects, in contrast, require extensive guidance from the brain, but probably utilize some of the spinal mechanisms that evolved earlier to control locomotion and scratching (Georgopoulos and Grillner, 1989). Postural control is an example of an intermediate behavior, relying heavily both on intrinsic spinal mechanisms and on descending control (Peterson et al., 1992).

This chapter deals specifically with voluntary arm movements. Implications of realistic arm, muscle, and spinal reflex properties for the control of double-joint arms have been investigated by many researchers (e.g., Feldman et al., 1990; Gribble et al., 1998; Jordan et al., 1994; Karniel and Inbar, 1997; Lukashin et al., 1996; Flanagan et al., 1993; Massone and Myers, 1996; van Dijk, 1978; Katayama and Kawato, 1993; van Sonderen and Denier van der Gon, 1990). A wide variety of arm-muscle-reflex models are used in these studies since there is no consensus as to what constitutes an adequate model or an appropriate level of abstraction (Winters and Stark, 1987). While these movements depend heavily on descending control signals, some of their important properties are attributable to spinal reflexes and to musculoskeletal mechanics (Houk and Rymer, 1981).

Our goal is to propose a mathematical model that captures the key complexities of the biological system while preserving a framework that is sufficiently abstract to facilitate computational studies of the overall control problem (see figure 1). One item of complexity that has been neglected in most past studies is the striking dependence of the stretch reflex on a low fractional power of velocity (Houk, 1981; Gielen and Houk, 1984). This nonlinearity produces a friction-like property in the stretch reflex that probably has a marked influence on voluntary movement control (Barto et al., 1999). The model also incorporates a Hill-

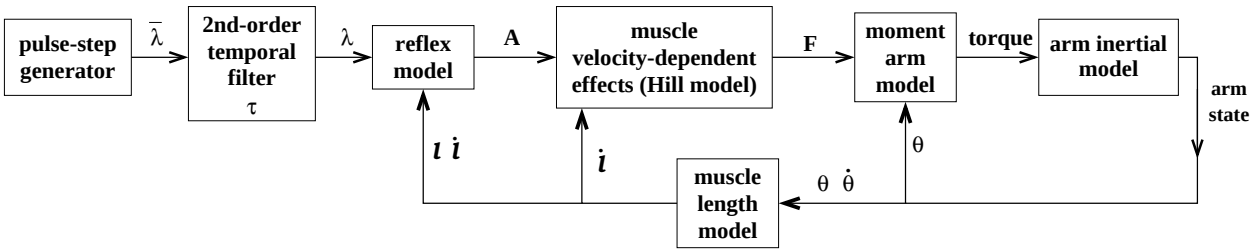

Figure 1: Model Architecture Overview. $\bar{\lambda}$ is the descending muscle motor command, λ is the tonic stretch reflex threshold, A is the motorneuron activation, F is muscle force, θ and $\dot{\theta}$ are joint position and velocity, and l and $\dot{l}$ are muscle length and stretch velocity, respectively.

based lumped parameter characterization of the muscle mechanics (Winters, 1990) and many features of the equilibrium-point theory of movement and arm geometry (Hogan et al., 1987; Bizzi et al., 1992; Feldman et al., 1990; Mussa-Ivaldi, 1992; Gribble et al., 1998).

The model architecture is outlined in figure 1. The arm model is composed of two joints (a simplified shoulder and an elbow), and moves in the horizontal plane. The arm is actuated by a set of six muscles; a simple model of muscular geometry produces variations as a function of skeletal configuration in the muscle's ability to produce torques about the joints. The current muscle length and stretch velocity provide significant influence (through the spinal reflex circuitry) on the muscle's ability to produce forces. A simple pulse-step generator is responsible for the production of the descending motor commands. This feed-forward control mechanism serves to illustrate the behavior and capabilities of the spinal-musculo-skeletal system, but it is not intended as a complete theory of voluntary motor control. In particular, we examine the stiction property of opposing muscles and focus on their participatory role in the production of braking antagonist pulses.

2 Musculo-Skeletal Geometry

Our skeletal model represents a human arm operating in a horizontal plane with two degrees of freedom: rotation of the shoulder and elbow (see figure 2). We use the standard equations of motion (e.g., Hollerbach and Flash, 1982) with the following parameters after Gribble et al. (1998): mass of upper and lower arm: 2.1 kg and 1.65 kg; length of upper and lower arm: 34 cm, 46 cm; moment of inertial about center of mass of upper and lower arm: .023 $kg{-}m^2$, .011 $kg{-}m^2$. Unlike some other models, the lower arm includes the hand,

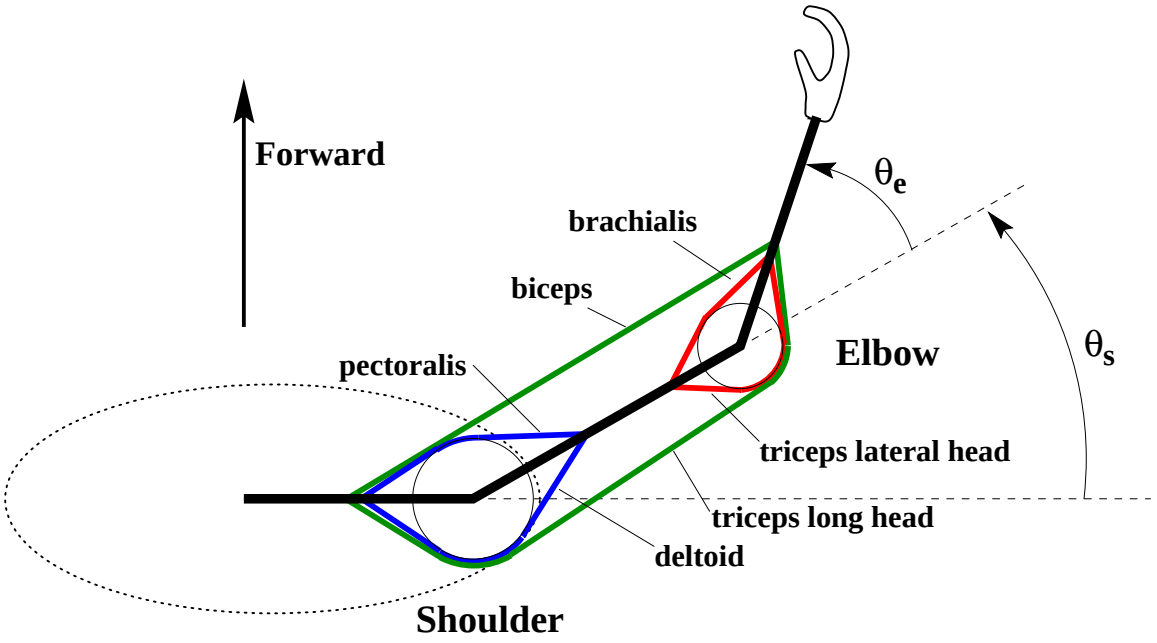

Figure 2: A schematic view of an idealized arm model with six muscles. $\theta_e = 0°$ (elbow orientation of 0°) is defined as full extension; $\theta_s = 0°$ is defined as the upper arm aligned with the sagittal plane of the body. The biceps and triceps long head produce moments about both the shoulder and elbow. The extensors are assumed to wrap around spherical joint capsules throughout the range of motion (resulting in constant moment arms). For the flexors, the muscles are assumed to leave the joint capsule at a critical flexion threshold, beyond which the muscles are modeled as following a straight path from origin to insertion. The origins and insertions depicted are not to scale.

although the wrist is assumed to be locked, which is appropriate for our studies of arm motion.

We lump the set of muscles acting on the arm into three pairs of equivalent muscles (e.g., Winters and Stark, 1988). One pair consists of a flexor and an extensor representing all the synergistic one-joint muscles for the shoulder, the actions of which are assumed to be dominated by the *pectoralis* and *deltoid*, respectively. A second pair of one-joint muscles model those acting on the elbow, which are assumed to correspond roughly to the *brachialis* and the *triceps lateral head*. The third pair represents flexor and extensor bi-articulate muscles spanning both joints, corresponding to the actions of the *biceps* and the *triceps long head*, respectively. The muscle moment arms for the extensors are set to 3.5 *cm* (shoulder

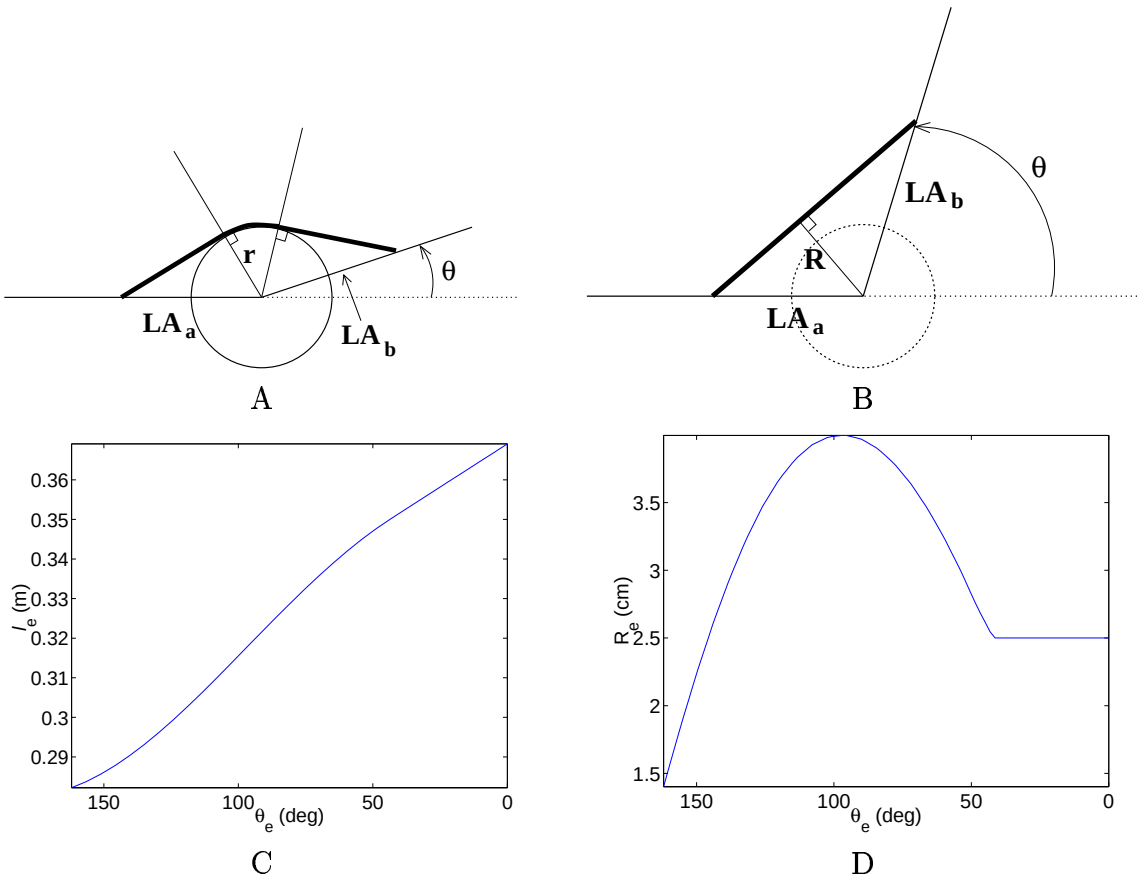

Figure 3: A simple muscle path model: wrapped path (A) and a straight path (B). Muscle path follows the dark curves. The critical parameters/variables are: θ (joint orientation, $\theta_e = 0^\circ$ = full elbow extension), LA_a and LA_b (distance from the center of joint rotation to muscle origin and insertion, respectively), r (the radius of the joint capsule), R (the muscle moment arm). This model has critical implications for both the muscle length (C) and the muscle moment arm (D) as the skeletal configuration changes.

extensor), 2.5 *cm* (elbow), 4 *cm* (biarticulate shoulder), and 2 *cm* (biarticulate elbow). The flexor moment arms are assumed to vary between 0 and 5 *cm*, depending upon the configuration of the arm.

Winters and Stark (1988) suggested a simple model of muscle path in which one assumes that for extended joint positions, the muscle wraps around a spherical joint capsule, resulting in a constant moment arm (figure 3A). However, when the joint flexes beyond a critical

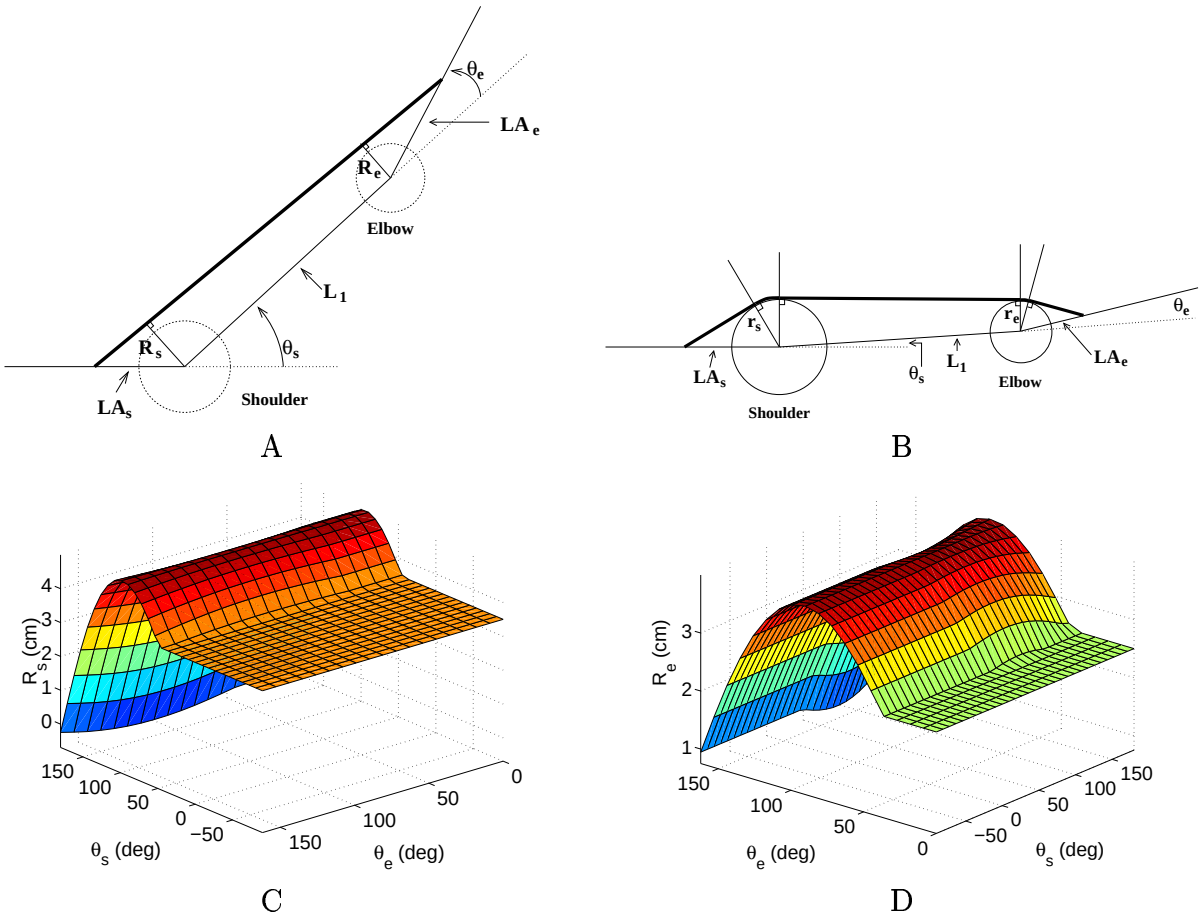

Figure 4: Two cases of the biarticulate muscle path model: A) no contact with the joint capsules, and B) contact with both joint capsules. Biarticulate moment arm as a function of joint angle for the shoulder (C) and elbow (B). θ_s and θ_e correspond to the joint angles for the shoulder and elbow, respectively; L_1, LA_1, and LA_2 represent the distance from shoulder to elbow joint, the distance from muscle origin to center of shoulder rotation, and the distance from muscle insertion to the center of elbow rotation; r_s and r_e are the joint capsule radii; and R_s and R_e are the moment arms for the shoulder and elbow. For the case illustrated in panel B, $R_s = r_s$ and $R_e = r_e$.

threshold, we assume that the muscle leaves the joint capsule and follows a straight path from origin to insertion (figure 3B). The result is a muscle moment arm that can be larger than the joint capsule, as is demonstrated in figure 3D. Note that for extreme flexion (where

$LA_a \neq LA_b$) the moment arm can also drop to a level below that of the joint capsule radius. The work of Amis et al. (1979) and An et al. (1981) indicates that this form of path model captures the primary variation of muscle moment arms as a function of joint orientation for a number of elbow muscles, including the *brachialis*. Less is known about the geometry of muscles involving the shoulder, and we assume for simplicity that this path model also applies in this case.

Little is also known about the geometry of the muscles that actuate two joints. We assume a generalization of the above model. In this case, the relationship between muscle path and joint configuration is more complicated as the muscle may wrap around either one, both, or neither of the joint capsules. The two extreme cases are shown in figure 4. The muscle moment arms as a function of joint configuration are demonstrated in figure 4C,D. Further details of derivation of the geometric muscle model, as well as the assumptions about the critical parameters (including joint capsule radii, and muscle origin/insertion locations) may be found in Fagg (2000).

3 The Tonic Stretch Reflex

As in the λ model of Feldman and colleagues (Feldman, 1966; Feldman et al., 1990), the neural control signal in our model determines the threshold muscle length, λ, for initiation of the tonic stretch reflex. Static force (zero stretch velocity), F, is generated as a function of the difference between a muscle's current length, l, and the current value of its λ, as plotted in figure 5A. Specifically:

$$F = K\ [l - \lambda]^+\ (1 - e^{-\frac{[l-\lambda]^+}{c}}), \tag{1}$$

where

$$[x]^+ = \begin{cases} x & \text{if } x > 0; \\ 0 & \text{if } x \leq 0. \end{cases} \tag{2}$$

The exponential term captures the initial recruitment of the motor units in a fashion that is related to the size principle (Houk et al., 1970; Binder et al., 1996). This term influences the force-length relationship most strongly at lengths just above the stretch reflex threshold λ. The parameter c determines the spatial extent of this influence. A short derivation is given in the Appendix, and the values used for the individual muscles are shown in table 1. As $[l - \lambda]^+$ increases, force due to the tonic stretch reflex approaches a linear function of length, with slope K (figure 5A). This parameter represents the stiffness of the tonic stretch reflex.

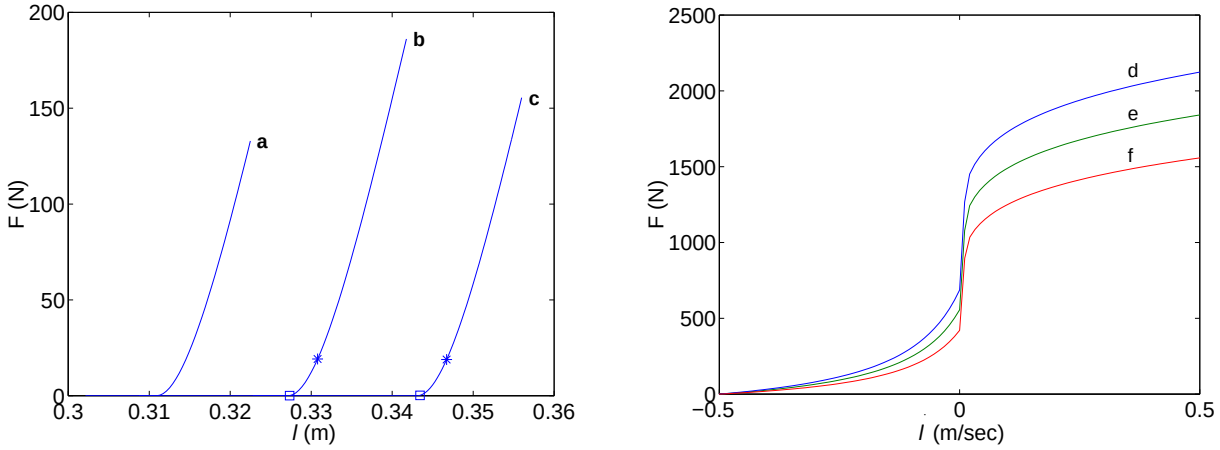

Figure 5: (A) Force as a function of muscle length for the simulated *brachialis*. It is assumed that the muscle is not stretching (i.e. $\dot{l} = 0$). a) $\lambda = 31.16\ cm$; b) $\lambda = 32.85\ cm$; c) $\lambda = 34.46\ cm$. The four marked points (two stars and two boxes) correspond to the same configuration and motor command as those indicated in figure 6A. (B) Force as a function of muscle stretch velocity ($\dot{l}$) for the simulated *brachialis*. $\dot{l} < 0$ corresponds to shortening of the muscle. $\lambda = 33.6\ cm$. d) $l = 36.28\ cm$; e) $l = 35.49\ cm$; f) $l = 34.68\ cm$.

The *normalized stiffness* of a muscle is defined as the stiffness of the stretch reflex normalized by the operating range of the muscle or joint. Houk and Rymer (1981) observed that across different muscles, normalized stiffness (K_n) tends to take on a constant value of about unity. This provides a convenient method by which reflex stiffness values may be computed from estimates of the operating range of muscle length and muscle force:

$$K = K_n \frac{\text{force range}}{\text{length range}}, \tag{3}$$

where *length range* is the change in muscle length from full extension to full flexion. We assume for our purposes that $K_n = 1$. Minimum force is assumed to be 0, thus *force range* is taken to be *max force*, which is often assumed to be linearly related to the muscle's Physiological Cross-Sectional Area (PCSA) (An et al., 1981). The derivation of this latter transformation is given in the Appendix. The muscle parameters and resulting reflex stiffnesses are shown in table 1.

The force-length behavior for a muscle is illustrated in figure 5A (muscle stretch velocity is 0). Changes in the descending motor command, λ, result in a shift of the force-length

Muscle	**PCSA** (cm^2)	**moment arm** (cm)	**length range** (cm)	**K** (N/m)	**H** $\left(\frac{sec}{m}\right)^{\frac{1}{5}}$	**c** (cm)
pectoralis	6.8 Freivalds (1985)	$3.5-(3.5)-5$	15.29	9022	0.61	1.56
deltoid	11.01 Freivalds (1985)	3.5	13.74	16251	1.10	1.41
brachialis	7.0 An et al. (1981)	$1.4-(2.5)-4$	8.91	15942	1.08	0.91
triceps lateral head	6.0 An et al. (1981)	2.5	7.85	15498	1.05	0.80
biceps	4.6 (short head + long head) An et al. (1981)	$0-(3.5)-5$ (s) $0.75-(2.5)-4$ (e)	22.86	4083	0.28	2.34
triceps long head	6.7 An et al. (1981)	4 (s) 2.5 (e)	23.56	5769	0.39	2.41
flexor carpi radialis	2 An et al. (1981)	2	4.71	8610	0.59	-

Table 1: Muscle parameters. Notation for variable moment arms: "minimum – (constant) – maximum", where *constant* refers to the constant moment arm size in the wrapping region. The parameters of the flexor carpi radialis are used in the appendix to derive a number of other model parameters.

curve along the length axis (to the left for decreasing values of λ; to the right for increasing values), as in the λ model (Feldman, 1966). The combined effect of all muscles acting on a single joint is derived by appropriately summing the corresponding force-length curves (e.g., Partridge, 1979), weighted by the muscle moment arm:

$$\tau_j = \sum_{m \in M_j} R_{j,m}(\theta)\, F_m(\theta, \lambda), \tag{4}$$

where τ_j is the torque exerted at joint j, M_j is the set of muscles which actuate joint j, $R_{j,m}(\theta)$ is the moment arm of muscle m about joint j, F_m is the force produced by the tonic stretch reflex for muscle m, and θ is the 2-element vector composed of the shoulder and elbow flexion angles. Note that we utilize the convention that $R_{j,m}(\theta)$ is positive if

the muscle generates joint flexion, and negative if it produces joint extension. We assume that the descending motor command affects both of the reflex thresholds (λ_{agonist} and $\lambda_{\text{antagonist}}$) by simultaneously increasing one as the other is decreased (or vice-versa). We also include a descending co-contraction signal (described in section 6), which is implemented as a simultaneous decrease in the two reflex thresholds. When λ_{agonist} and $\lambda_{\text{antagonist}}$ are selected in such a way that both muscles are tonically active, equation 4 defines a force field with a unique equilibrium position (Hogan et al., 1987; Bizzi et al., 1992).

The combined effect of the four equivalent muscles acting on the elbow joint is shown in figure 6A. The curves illustrated in the figure demonstrate the position-dependent, isometric torque response of the set of muscles under three different constant motor commands. The motor commands were selected under the same conditions as those produced by subjects of the Astryan and Feldman (1965) experiment (the results of which are shown in panel B). A specified level of torque is established against a load at a specified elbow position (each indicated by one of the three circles in panel A). This is accomplished with the model by setting the elbow to the desired position, and then shifting λ's together until the desired torque is achieved. Redundant degrees of freedom are resolved by constraining the equilibrium position of each agonist/antagonist pair (brachialis/triceps lateral head, and biceps/triceps long head) to be the same joint position and by enforcing a small amount of overlap in the tonic reflex region for each pair (i.e., each pair is slightly co-contracted).

The curve emanating from each of the circles is produced by holding the motor commands constant as the elbow is allowed to flex. The resulting muscle-produced torque is thus equal in magnitude, but opposite in direction to the opposing isometric load at that joint location. In other words, if the opposing load were suddenly reduced from its initial level (at the circles) to some lower magnitude, the curves indicate the position to which the elbow would equilibrate (assuming no changes in the descending motor commands). The precise shape of the iso-motor command curves is determined by a combination of force-generation ability of the tonic stretch reflex, and the position-dependent variation in muscle moment arm. The difference in slope in curves **b** and **c** results from the increase in moment arm due to a lifting of the muscle off of the joint capsule. The contribution of the nonlinearity of the stretch reflex versus the moment arm variation becomes clearer by comparing the corresponding points in figures 5A and 6A (the points are marked with stars or boxes in the two figures). Furthermore, figure 6C shows the elbow torque response over a wider range of the variables. The change in slope of the iso-motor command curves is a direct result of the variation in muscle moment arms for the elbow flexors. The constant slope of these curves in the $\tau < 0$ region is due to our assumption of constant moment arms for extensors. This assumption roughly approximates the experimental observations of Amis et al. (1979) regarding the elbow joint and is consistent with the assumptions made by the models of Astryan and

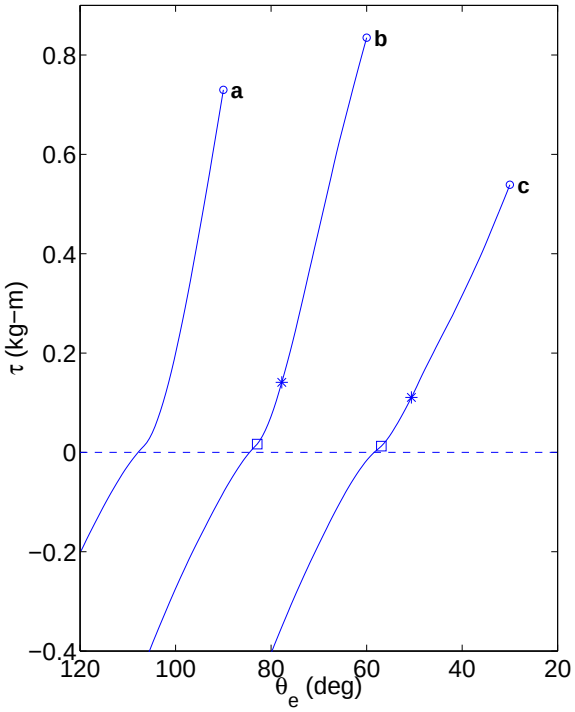

A

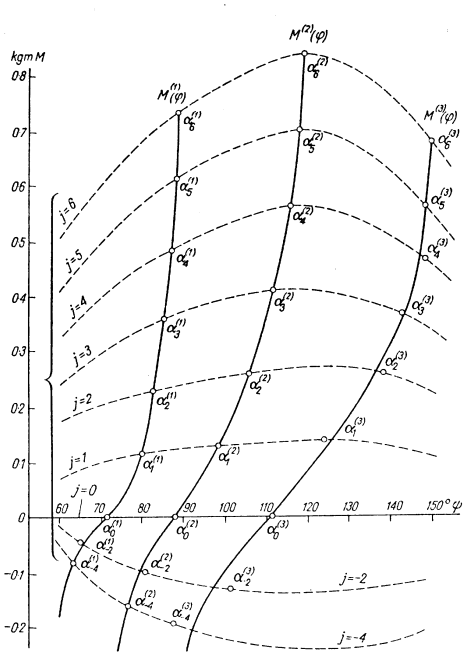

B

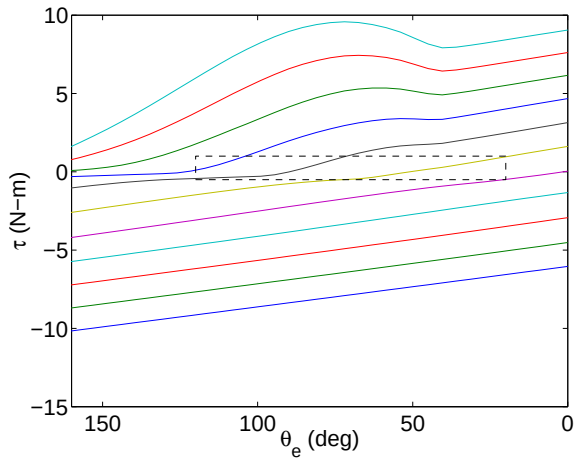

C

Figure 6: (A) Torque as a function of elbow position (θ_e) for three levels of constant motor command. Elbow position is in the coordinate system of our model, with $\theta_e = 0$ corresponding to full elbow extension. (B) Observed torque as a function of elbow position (reprinted from Astryan and Feldman, 1965). Note that $\psi = 180 - \theta_e$. (C) Torque as a function of elbow position (θ_e). Data taken under the same conditions as in panel A, except that a wider region of state space and descending motor commands are shown. The dashed box indicates the same region of space as in panel A.

Feldman (1965) and Gribble et al. (1998).

4 Fractional Power Damping

Our model of muscle and spinal reflex properties also includes significant velocity-dependent components. As in the λ model and the muscle-reflex model of Wu et al. (1990), the force-velocity-length relation includes the effects of reflex-induced EMG activity, which particularly influences the relation for positive velocities (lengthening). For negative velocities (shortening) we ignore stretch reflex velocity dependence, where it has considerably less effect on force generation (Gielen and Houk, 1984). Instead, the variation of force production with shortening velocity is assumed to be dominated by muscle mechanical properties. In contrast, the velocity dependence of lengthening responses is modeled as the combined result of muscle mechanics and the stretch reflex (Houk, 1981; Gielen and Houk, 1984). We also adopt the well-supported approach of multiplicatively combining length- and velocity-dependent muscle mechanical characteristics (Winters, 1990; Wu et al., 1990).

Combining the approach of Gribble et al. (1998) and Wu et al. (1990), we define muscle activation at time t to be:

$$A = [l - \lambda + Hr]^+ . \tag{5}$$

The terms $l - \lambda$ and Hr, respectively, represent the static and dynamic components of reflex produced activation, where H is a gain coefficient for the dynamic component. The values used for specific equivalent muscles are given in table 1. The reflex related damping term, r, is defined as follows:

$$r = \begin{cases} \left[\dot{l}^{1/5}\,(l - \lambda + \mu)\right]^+ & \text{if } V < \dot{l} \text{ (fast lengthening);} \\ \left[V^{1/5}\,\frac{\dot{l}}{V}\,(l - \lambda + \mu)\right]^+ & \text{if } 0 \le \dot{l} < V \text{ (slow lengthening);} \\ 0 & \text{otherwise (shortening),} \end{cases} \tag{6}$$

where $V = 1.25\ cm/sec$ is a stretch velocity threshold separating the "fast" and "slow" lengthening regions, and $\mu > 0$ represents the receptor's baseline positional sensitivity (described below).

The rationale for this definition of the dependence of muscle activation on stretch velocity follows Wu et al. (1990). In ramp stretch experiments with the human wrist, Gielen and Houk (1987) estimated power law relationships for EMG activity and force response to have exponents of approximately 1/3 and 1/5, respectively. Modeling studies (Houk, 1981; Gielen and Houk, 1984) suggest that the smaller exponent for force results from the combination of muscle mechanical properties and reflex-produced neural input during muscle

lengthening. For mathematical convenience in the FPD model, we use the 1/5 exponent to define the velocity-dependent muscle activation during lengthening. However, the slope of $\dot{l}^{1/5}$ approaches infinity as $\dot{l}$ approaches 0, which results in numerical instabilities in the model. This difficulty is solved by introducing a short, linearly-varying region in the range $0 \leq \dot{l} < V$ (corresponding to the "slow lengthening" component of equation 6). Following the results of Houk et al. (1970), which indicate a small contribution of tendon organ feedback to motorneuron activity, a tendon organ contribution to muscle activity is not explicitly included in the model (c.f., Houk and Rymer, 1981).

Setting the parameter μ in equation 6 to be greater than zero allows reflex activity when the muscle length is below the threshold λ of the tonic stretch reflex, provided that the muscle is lengthening. It therefore has an effect similar to that of parameter μ of Gribble et al. (1998), and x_{p0} of Wu et al. (1990). We choose $\mu = 0.028\ m$, which falls within the upper range estimated by Wu et al. (1990).

In the dynamic case, equation 1 is expanded to include velocity-dependent muscle activation and muscle mechanical effects. Specifically,

$$F = K\ A\ \left(1 - e^{-A/c}\right)\ m\left(\dot{l}\right), \tag{7}$$

where

$$m(\dot{l}) = \begin{cases} \left[(b + a\dot{l})/(b - \dot{l})\right]^{+} & \text{if } \dot{l} \leq 0 \text{ (shortening);} \\ 1 & \text{otherwise (lengthening),} \end{cases} \tag{8}$$

and where a and b are the Hill equation parameters (Hill, 1938). K and c are the reflex stiffness and reflex threshold transition parameters, respectively (as defined for equation 1). Although $m(\dot{l}) = 1$ appears to imply that there is no drop in force production with a positive stretch velocity, these effects are actually accounted for by the choice of 1/5 fractional power of equation 6.

For muscle shortening, equation 8 captures the Hill equation in which the maximum shortening velocity, v_{max}, is $-b/a$. The FPD model incorporates the simplest assumption that v_{max} remains constant over muscle length and activation level. Winters (1990) discusses implications of this assumption, which we consider to be minor for our purposes. Also for simplicity, we assume that a and b are the same for all the model's muscles, although these parameters would vary as a function of muscle fiber length in a more detailed model. We set $a = .25$ following Winters (1990). The value for b is determined by averaging the values for v_{max} given by Winters and Stark (1985) in radians per second. Assuming a constant moment arm of 2.0 cm yields $v_{max} = -.5\ m/s$, or $b = .125$.

We assume that the non-linear damping gain, H, is proportional to a muscle's stiffness, K. Gielen and Houk (1984) reported a force relationship to velocity for stretching of the wrist flexor muscles described by the following equation:

$$F - F_0 \;=\; C_1 v^{1/5}(x - x_{01}),$$

where F is the force produced against the manipulandum, F_0 is force prior to stretch, v is the velocity of manipulandum movement, x is the current manipulandum position, and x_{01} represents the combined effects of λ and μ in equation 6. In the FPD model, KH corresponds to C_1, for which Gielen and Houk (1984) estimated a value of approximately $955\frac{N}{m}(\frac{sec}{m})^{1/5}$. In this experiment, length (m) was measured in the coordinate system of the manipulandum, which had a moment arm of approximately 4 times that of the wrist-actuating muscles. Thus, for our purposes:

$$C_1 = 955 \times 4 \times 4^{1/5} = 5040.5 \; \frac{N}{m} \left(\frac{sec}{m}\right)^{1/5}.$$

If we assume a stiffness of $K = 12069 \; N/m$ for the muscles involved in wrist flexion (a quantity that is derived in the Appendix), then H_{fcr} , the lumped gain parameter for the wrist flexion muscles[1], is defined as follows:

$$\begin{aligned} H_{fcr} &= \frac{C_1}{K} \\ &= 5040.5 \; \frac{N}{m} \left(\frac{sec}{m}\right)^{1/5} \frac{1 \; m}{8610 \;\; N} \\ &= 0.59 \; \left(\frac{sec}{m}\right)^{1/5}, \end{aligned} \tag{9}$$

where the damping gain parameter for any particular muscle (H_i) is related to the muscle's stiffness relative to the flexor carpi radialis:

$$H_i \;=\; H_{fcr} \frac{K_i}{K_{fcr}}.$$

The resulting parameters which were used in the model are given in table 1.

As described above, experimental results suggest that EMG activation varies as a 1/3 fractional power of stretch velocity (Houk, 1981; Gielen and Houk, 1984). When relating model behavior to EMG data, we utilize a modification of equation 5, in which the 1/5 fractional power (of equation 6) is replaced with 1/3 power. Note, however, that this formation

[1]We assume an equivalent muscle corresponding to the *flexor carpi radialis*.

omits the initial burst-phase of spindle responses to stretch (Hasan and Houk, 1975; Houk et al., 1992). Specifically:

$$EMG = \begin{cases} \left[l - \lambda + H \left[\dot{l}^{1/3} (l - \lambda + \mu) \right]^+ \right]^+ & \text{if } V < \dot{l}; \\ \left[l - \lambda + H \left[V^{1/3} \frac{\dot{l}}{V} (l - \lambda + \mu) \right]^+ \right]^+ & \text{if } 0 \leq \dot{l} < V; \\ [l - \lambda]^+ & \text{otherwise.} \end{cases} \tag{10}$$

The velocity dependent effects of the Hill equation for muscle shortening and the Gielen-Houk stretch reflex non-linearity are illustrated in figure 5B. The three curves represent different constant muscle lengths. As shortening velocity approaches V_{max} ($-0.5\ m/s$), force generation ability drops to 0 N in all cases. With muscle stretch, there is an initial rapid increase in the response force. The slope of this response drops as stretch velocity increases.

The combined effect of static and dynamic components is illustrated in figure 7. In this case, $\lambda = 0.323\ m$; changes in λ shift the surface along the length axis. An important feature of this surface is that for any fixed stretch velocity, force (F of equation 7) approaches a linear function of l whose slope increases with increasing $\dot{l}$. This results from the $l - \lambda$ term that appears in both the definition of muscle activation, A (equation 5), and the definition of spindle activation, r (equation 6). Note that although the reflex threshold is set to $0.323\ m$, during stretch, activation onset occurs much earlier (about $0.315\ m$ in figure 7). This effect is due to the additive combination of the position- and velocity-sensitive muscle spindles in equation 5.

5 FPD Interaction of Multiple Muscles

A critical feature of the force-length-velocity curve of figure 7 is the sudden increase in response force as the system transitions from zero stretch velocity to a small degree of stretching. At the initiation of a muscle stretch, this immediate response is due to the large short-range mechanical elasticity of the muscle, which is then followed by a delayed reflex response (Houk, 1981; Houk et al., 1981). However, the characterization captured by equations 5 and 6 lumps the two components together, allowing a simpler mathematical specification.

When the reflex thresholds for an agonist/antagonist muscle pair are set such that both muscles are simultaneously active, then the result is a region of *stiction* that surrounds the equilibrium position in the force field produced by the muscle pair. This stiction region is characterized by a rapid change in the torque response with either a positive or negative deviation from zero stretch velocity. This is demonstrated in figure 8, which shows the torque

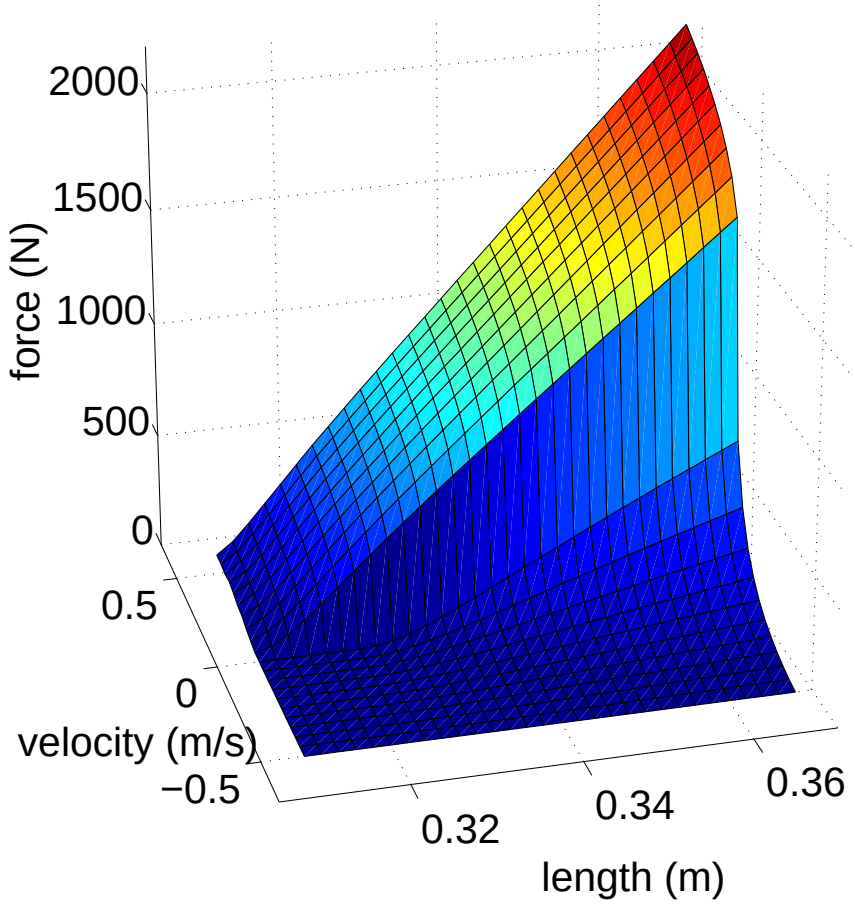

Figure 7: Force as a function of muscle length (l) and velocity ($\dot{l}$) for both shortening and lengthening with $\lambda = 0.323\ m$. Positive velocity corresponds to muscle stretching.

response as a function of elbow position and velocity assuming a constant set of descending motor commands. The reflex thresholds are set such that the joint equilibrium position is 90°, which corresponds to the center of the ellipse. The region corresponding to low joint position values and negative joint velocities is the stretch region for the flexors acting on the elbow, which produce a large positive torque. The dark, thick, "S-shaped" curve indicates where torque $\tau = 0$. The hashed line is where $\dot{\theta} = 0$ (the tonic torque reflex response).

Joint positions near the equilibrium are such that small negative joint velocities (joint extension/stretch of the elbow flexors) result in a large, opposing response torque (ellipse

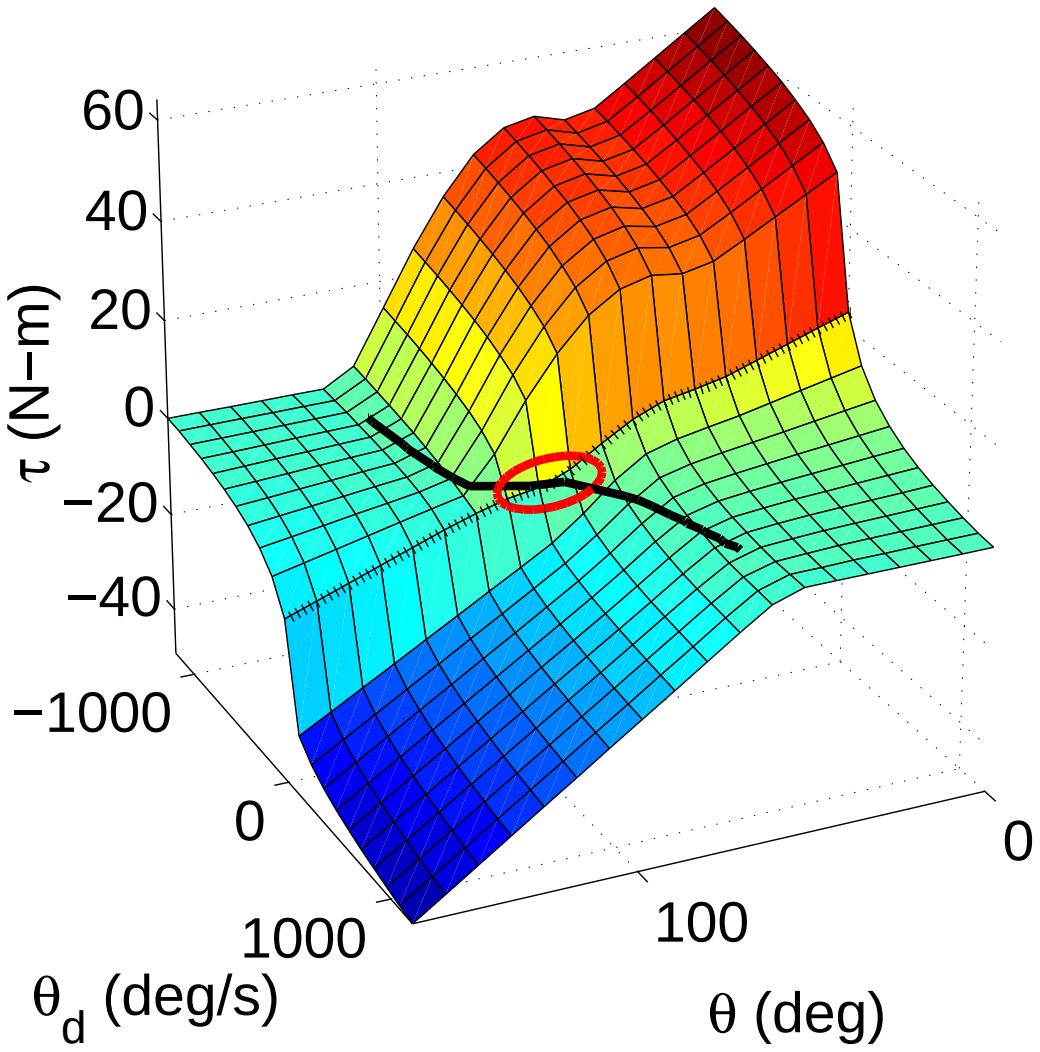

Figure 8: Elbow torque as a function of configuration of the elbow (θ) and its velocity ($\dot{\theta}$). The action of four muscles contribute to the total torque. $\theta = 0$ corresponds to full extension of the elbow. The shoulder is held at a fixed position. The dark, thick, "S-shaped" curve indicates where torque $\tau = 0$; the ellipse indicates the stiction region. The equilibrium position of the joint is located in the middle of the stiction region (90°).

region of figure 8). Positive joint velocities also result in a large opposing response torque. When the joint state approaches the equilibrium (within about $+/-20^\circ$ from the target at 90°), this combination of opposing forces has the effect of very quickly driving the joint velocity to a very small level. When this happens, although the joint continues to move very slowly toward the equilibrium, behaviorally, the joint effectively stops moving (or "sticks") at the point at which it entered the stiction region. Once within this region, the joint requires a significant perturbation or shift in equilibrium position in order to be dislodged. The result is a system that does not exhibit significant ringing near the equilibrium (Barto et al., 1999).

Far away from the equilibrium position, this stiction property does not hold. Although there is a significant response torque for deviations from 0 velocity in one direction, an opposite response does not exist for deviations in the other direction. In fact, the response torque does not change sign, as it does within the stiction region.

Figure 9 shows the phase plane dynamics corresponding to the torque surface shown in figure 8. Each arrow indicates the direction and magnitude of the evolution of the system given the state corresponding to the tail of the arrow. The bold curve is the velocity nullcline ($\ddot{\theta} = 0$). Note that this set of points differs from that of figure 8 in which $\tau = 0$; the velocity nullcline includes forces in addition to those produced by the muscles (including inertial, coriolis, and externally-induced forces). The upper right and lower left quadrants of figure 9 correspond to the regions of state space in which the flexor and extensor muscles (respectively) respond to stretch by producing large forces. As seen in the figure, these forces result in a rapid reduction in velocity.

In the model, one class of motor commands (described below) causes the equilibrium positions of muscle pairs to shift together. This has the effect of shifting the entire surface of figure 8 along the joint position dimension. Co-contraction of muscle pairs has the effect of bringing the two stretch reflex regions closer together along the position dimension, thus increasing their overlap. This results in an increase in the width of the stiction region.

6 Responses to Voluntary Commands

Arm movements are controlled in the model by producing time-varying motor commands (λ_m's) that descend to the spinal cord. One of the simplest representations of such a time varying behavior is the pulse-step motor command. This form of motor command description is well established in the saccadic eye movement literature (Robinson, 1975), and has been suggested as a reasonable approximation for the control of voluntary limb movements (Ghez, 1979; Ghez and Martin, 1982). The pulse-step waveform describes the time course of the reflex thresholds for an opposing pair of muscles. Hence, we can think of the waveform as specifying the equilibrium position of the joint, with the pulse playing the role of move-

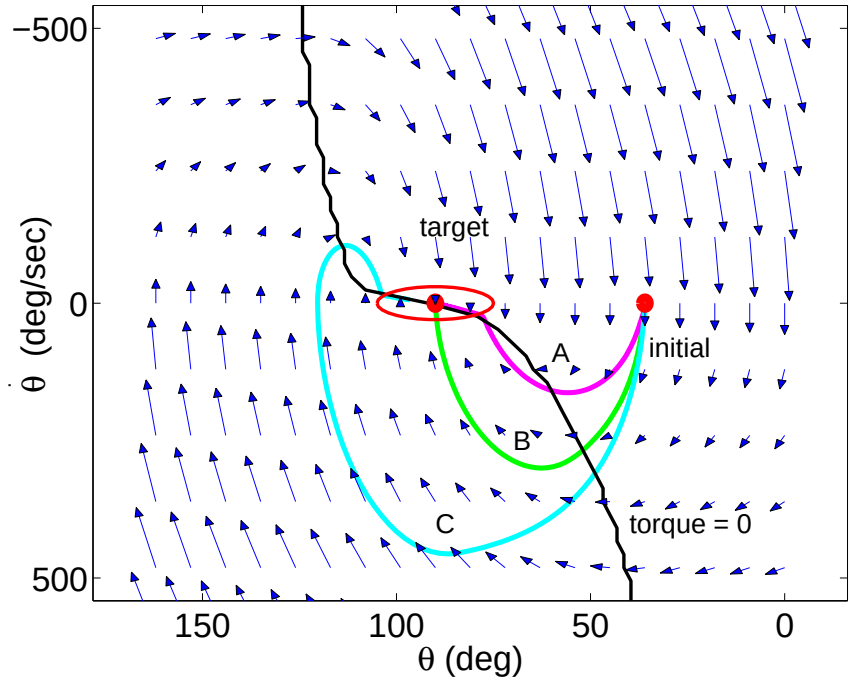

Figure 9: Phase plane dynamics for the elbow joint. The arrows indicate the direction and magnitude of the evolution of the elbow state (θ and $\dot{\theta}$). The bold, S-shaped curve represents the velocity nullcline ($\ddot{\theta} = 0$). The muscle motor commands are such that the equilibrium point is at 90°, which falls in the center of the ellipse indicating the stiction region. Three paths (emanating from the *initial* position at 36°) show the evolution of elbow state for three different movement trials, in which different motor commands are utilized (these are described in section 6). Path A corresponds to the case in which the equilibrium position is shifted to the target without first executing a pulse. In this case, the elbow effectively falls short of the target. Path B is one in which the pulse magnitude and duration are such that the elbow stops at the target. Path C is one in which the pulse magnitude is too large, resulting in an overshoot of the target.

ment initiation, and the step indicating where the movement should stop. However, unlike other equilibrium point theories, simply setting the step to the target joint location in the FPD model does not guarantee that the joint will arrive there in a reasonable amount of time (Barto et al., 1999). Instead, due to the stiction property around the equilibrium, the joint may effectively stop at a point that is not the equilibrium. As a result, it is necessary

to specify the properties of the pulse (height and duration) such that the joint sticks at the desired target.

In addition to specifying the timecourse of the equilibrium position, it is also possible to superimpose a co-contraction signal which causes an overlap in the tonic muscle response of the opposing muscle pair. For simplicity, here we will assume that a constant non-zero level of co-contraction is specified prior to and during the entire movement.

For the case of a single opposing pair of muscles, the individual reflex thresholds ($\bar{\lambda}_{flexor}$ and $\bar{\lambda}_{extensor}$) are expressed as follows:

$$\bar{\lambda}_m(t) \;=\; CC + \begin{cases} L_m(\theta_I) & \text{if } t < 0; \\ L_m(\theta_T) + D_m\, P & \text{if } 0 <= t < S; \\ L_m(\theta_T) & \text{if } S <= t, \end{cases} \tag{11}$$

where CC is the co-contraction level used throughout this example; $L_m(\theta)$ is the commanded length of muscle m at the corresponding elbow joint angle, θ; θ_I, and θ_T are the equilibrium positions for the initial and target positions, D_m is the direction of muscle pull ($+1$ for flexor, and -1 for extensor); P is the pulse magnitude; and S is the time of transition from pulse to step.

The muscle pulse-step waveforms ($\bar{\lambda}_m$'s) are made less abrupt by temporally filtering them through a cascade of two low-pass filters, each with a time constant of 40 ms (Engelbrecht, 1999). Miller and Sinkjaer (1998) suggest that such a form of temporal filtering may be the result of the time required to recruit a large set of cortical motorneurons and their associated interneurons. The result is a set of motor signals (λ_m's) representing the spinal reflex thresholds of equations 5-10. Note that this form of motor program does not allow for the on-line adjustment of the descending motor signals. Instead, the parameters are selected a priori, and the motor commands are executed in a completely open-loop manner. Thus, our use of a pulse-step waveform should not be viewed as a complete theory of limb motor control. Instead, this mechanism should be seen as a technique for "exercising" the plant model, which incorporates skeletal, muscular, and spinal mechanisms.

For the results that follow, the experimental paradigm is one in which the shoulder is held in a fixed position ($\theta_s = 90°$), and the model is asked to generate point-to-point movements of the elbow. Because both mono- and bi-articulate muscles are involved in production of elbow movement, we are faced with an additional level of redundancy. For simplicity, CC, P, and S are chosen to be the same for both pairs of muscles acting on the elbow.

Figure 10 demonstrates the behavior that results from the execution of three different pulse-step waveforms. Each of the three movements start with the elbow at 36°. The target is set to 90°. We selected $CC = 0.015$ for all three pulse-step waveforms, which yields a movement duration of about 300 ms for the accurate reach (panel B). For each of the three

cases, five sub-panels are shown. The first two sub-panels (top) demonstrate the timecourse of the elbow joint angle and angular velocity, respectively. The third sub-panel shows the stretch reflex threshold (λ_m) for the mono-articulate flexor (agonist). The fourth sub-panel illustrates the timecourse of the EMG signals for the mono-articulate flexor (positive deviation) and extensor (negative deviation). EMG magnitude for the corresponding muscle is read as the height of the shaded region. The final sub-panel indicates the muscle-induced torques that result from the descending motor commands.

Figure 10A shows the case in which no pulse is executed ($S = 0$). The result is a movement which undershoots the target by more than 12°. Once the elbow movement slows down to a low velocity at about 600 ms, it enters the elbow stiction region. Once there, it maintains a very slow creep toward the equilibrium position. Even after an additional 400 ms, the elbow is still about 5° from the target. Thus, for all intents and purposes (certainly on a behavioral time scale), the movement has effectively stopped at 600 ms. The corresponding phase plane behavior is shown in figure 9 (path A). The path obtains a low magnitude peak velocity, and enters the stiction region on the right-hand side of the target position.

The descending motor command (middle sub-panel of figure 10A) shows a decrease in the stretch reflex threshold for the mono-articulate flexor. There is a simultaneous increase in the threshold for the extensor that is not shown. The result is a shift in the equilibrium position from the initial position to the target. The gradual transition from the initial position ($\lambda_m = 33.6\ cm$) to the target ($\lambda_m = 31.1\ cm$) is due to the temporal filtering in the pulse-step waveform (see figure 1). The reduction in the flexor threshold results in a reflex-induced increase in the EMG activity of the flexor. The opposite effect is seen in the extensor EMG. The combined effect is a net positive torque produced by the muscles, which initiates an elbow flexion movement.

The transition to the braking phase of movement is the result of two distinct components (from equation 5): 1) the movement of the elbow increases the length of the extensor, increasing the tonic response of the stretch reflex, and 2) this response is further facilitated by the dynamic response of the stretch reflex. Thus, prior to reaching the target, the torques induced by the extensor overcome those of the flexor, resulting in a net negative (or slowing) torque. After the movement settles to a low velocity, the residual EMG activity in both the flexor and extensor is primarily the result of the descending co-contraction signal.

When a pulse is introduced with appropriate parameters ($S = 50\ ms$ and $P = 0.065$), the elbow completes its motion exactly at the target (figure 10B, and path B of figure 9). The direct effects of the pulse are seen in the trace of the muscle motor command (middle sub-panel). Compared to the case in which no pulse is executed, these thresholds temporarily achieve a higher deviation from the target step level. This difference leads to an even higher level of EMG activity for the flexor, which results in a higher acceleration of the elbow, and

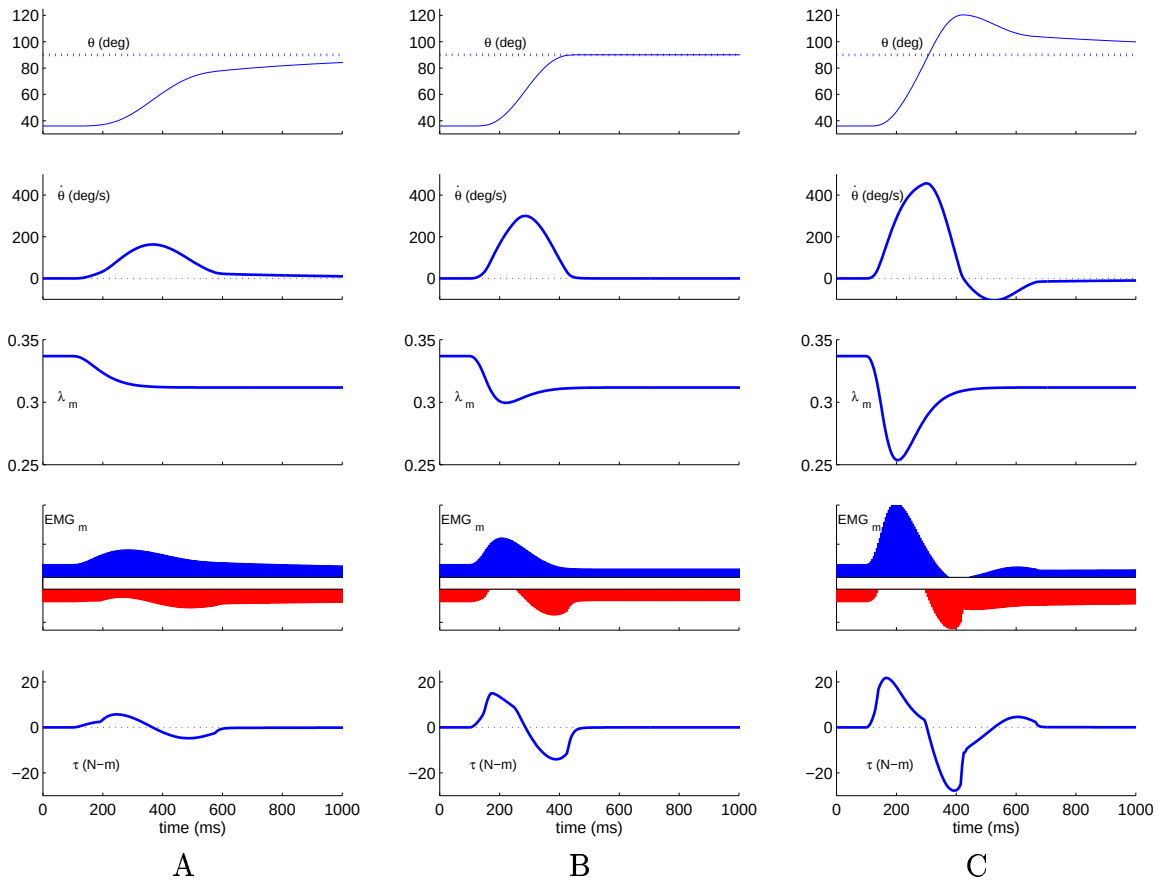

Figure 10: Behavioral patterns which result from executing three different pulse-step waveforms: A) Execution of a step only (the equilibrium point is shifted directly from initial to target positions; B) Execution of a pulse-step which brings the elbow directly to the target position; and C) Execution of a pulse-step which results in an overshoot of the target. The vertical sub-panels show the timecourses of the following: elbow position, elbow velocity, muscle motor command for the mono-articulate flexor, simulated EMG activity for the brachialis (dark region) and triceps lateral head (light region), and the muscle-produced torque. Magnitude of EMG activity is indicated by the height of the shaded regions. The activity of the brachialis (the flexor) is shown as a deviation in the upward direction; the activity of the triceps lateral head (extensor) is shown as a deviation in the downward direction.

hence an increase in peak velocity. Because the elbow obtains a higher velocity than the step-only case, the extensor stretch velocity is higher, leading to an increase in the dynamic response of the antagonist stretch reflex. This results in a larger braking response of the extensor muscles.

In the case in which the pulse magnitude is set even higher ($P = 0.2$), the elbow overshoots the target (figure 10C). As seen in the phase portrait (figure 9, path C), the path completely passes the stiction region. As a result, the elbow begins to move in the opposite direction. However, this re-acceleration is limited: the resulting stretch of the flexor induces a second agonist burst, which again slows the elbow, causing it to fall into the stiction region (this time, the left-hand side of the target position). Note that in the phase plane, the second velocity peak corresponds (by definition) to the path's crossing of the velocity nullcline ($\ddot{\theta} = 0$). The reason that the first velocity peak does not occur at the pictured nullcline is that at the time of the peak, the descending motor signals do not correspond to the target, but instead to the target "plus pulse" (with temporal smoothing). Thus, at the time of the first velocity peak, the nullcline is actually shifted to the left of where it is depicted in figure 9.

The torque profile for the overshoot case shown in figure 10C (the fifth sub-panel) contains two sharp changes in slope at about 300 ms and 430 ms. These points correspond to the onset and offset of the antagonist muscle burst. It is important to note that although the descending motor signals (the λ_m's) specify the time of transition to the step, and the step level itself, the precise onset time and magnitude of the antagonist braking pulse is determined by the current state of the arm (θ and $\dot{\theta}$). Even when the descending command remains the same on a different movement trial, if the phase plane evolution of the arm shows any differences (e.g., due to external loading), then this will be reflected as a difference in the antagonist burst pattern.

7 Discussion

This chapter focuses on the development of a neuromuscular model that captures a tradeoff between the key complexities of the biological system and the preservation of an abstract framework that facilitates efficient simulation of the model. In particular, it is important to take into account certain properties of the muscle mechanics and the spinal reflex circuitry. To that end, our model represents a synthesis of equilibrium point approaches (e.g., Feldman, 1966; Bizzi et al., 1982; Feldman et al., 1990; Gribble et al., 1998), theories of velocity-dependent force generation of muscle (Winters and Stark, 1988; Winters, 1990), and theories of stretch reflex-induced non-linear damping (Gielen and Houk, 1987; Wu et al., 1990).

In equilibrium point theories of motor control, when two opposing muscles are activated to a sufficient degree, the spring-like dynamics of the muscle pair creates a potential well that contains a unique joint equilibrium position (Feldman, 1966; Bizzi et al., 1982; Hogan, 1984). In *these models*, the establishment of the potential well results in a movement of the joint, which ultimately comes to rest at the equilibrium point. By altering the relative activation of the opposing muscles, it is possible to alter the location of the equilibrium. Thus, a movement from one point to another can be achieved by shifting the joint equilibrium position from the initial point to the target location (Gribble et al., 1998; Mussa-Ivaldi, 1997).

Muscle stretch studies in the cat soleus muscle (Nichols and Houk, 1976) and the human wrist (Gielen and Houk, 1984) suggest that the stretch reflex plays a critical role during lengthening in not only the maintenance of muscle stiffness (implicitly assumed in the equilibrium point models), but also in the production of a damping force that is nonlinearly related to the velocity of stretch (Houk, 1981). These ideas have been further elaborated in the models of Hasan (1983), Gielen and Houk (1987) and Wu et al. (1990), and have also proven to be useful in artificial control problems (Wu et al., 1997; Chang et al., 1999).

Ghez and Martin (1982) have shown that both the antagonist and second agonist muscle bursts during reaching movements in cat are suppressed when the limb is prevented from moving. These results imply a significant role of the stretch reflex in the production of these latter bursts. The head movement study of Hannaford and Stark (1985) indicates that the triphasic muscle burst pattern occurs primarily during rapid head movements (those which are nearly time-optimal). Subsequent modeling work shows that reflex action can be used to derive the timing and magnitude of the braking (antagonist) and clamping (second agonist) muscle bursts (Ramos and Stark, 1987; Ramos et al., 1989). Similar to our model, they observe that an occurrence of the second agonist burst is contingent upon an overshoot by the joint of the final resting position. Although both models include a Hill-type nonlinearity for muscle shortening, the Hannaford and Stark (1985) model utilizes a linear response of the stretch receptor to velocity. Furthermore, the Hannaford and Stark (1985) model assumes that the stretch reflex is not involved in shaping muscle activation during the initial muscle burst. In contrast, our formulation of the interaction between descending command and reflex activation is more straightforward in that both components are assumed to contribute to muscle activation at all times.

Lin and Rymer (1998) recently examined the contribution of damping by the stretch reflex in a preparation composed of a single muscle and a simulated inertial load. They observed that inclusion of the stretch reflex led to lightly damped oscillations of the simulated mass, and not the stiction-like behavior that is observed in our model. However, it is important to note that the stiction property requires the co-activation of a pair of opposing muscles, and only holds near the equilibrium position (section 5). Without the second muscle, energy is removed only during one half-cycle of the oscillation (the stretch of the remaining muscle).

Thus, multiple cycles will be required before the system comes to rest, which is consistent with the Lin and Rymer (1998) experimental results.

Our theory has much in common with equilibrium point theories of motor control since an equilibrium point is specified, but the effective movement endpoint depends on the equilibrium point in a complex way that involves the dynamics of the arm (with spinal contribution) in a neighborhood around the equilibrium point (Wu et al., 1990; Barto et al., 1999). A consequence of FPD-induced stiction behavior is that the central motor system may not simply rely upon a shifting of the equilibrium position from the initial to the target position. Ghez (1979) and Ghez and Martin (1982) suggest that neural commands that control limb movements in cat appear to be comprised of a high-magnitude (pulse) component, followed by a smaller step component Gielen and Houk (1986). Although analogous to the pulse-step commands that control rapid eye movements (Keller and Robinson, 1971; Robinson, 1975), our model relies on the stretch reflex to brake the ongoing movement, rather than relying on the intrinsic viscous behavior of the arm. Furthermore, in our model, the pulse has the function of moving the joint out of the stiction region, allowing the joint to achieve a non-trivial velocity before it arrives to the new stiction region specified by the step command corresponding to the target.

Our model is similar to that of Karniel and Inbar (1997), in that it relies upon the natural dynamics of the arm and muscles in order to achieve realistic kinematic trajectories while specifying the control in terms of a feedforward pulse-step motor command waveform. Such a representation constitutes a simple description of the time-varying motor command as compared with, for example, a continuous representation of torque output as a function of time (e.g., Katayama and Kawato, 1993). However, in the model of Karniel and Inbar (1997), the parameters are separately specified for the agonist and antagonist muscle bursts. In contrast, Lestienne (1979) suggests that these bursts are not separately planned, but instead are planned as a unit. Because our model relies on the stretch reflex for the on-line production of the braking antagonist muscle burst, we are in fact providing an explicit mechanism for pairing agonist and antagonist bursts. When the limb is externally loaded (e.g., with viscous, inertial, or elastic loads used in the experiments of Gottlieb, 1996), it will follow a different path through phase space. Because the reflex formulation is sensitive to a complex combination of muscle length and stretch velocity, this will affect the magnitude and timing of reflex-mediated antagonist response, even if the descending control parameters relating to the braking phase (co-contraction and step in our pulse-step formulation) are identical across the different loading conditions. Hence, the pairing process is not one that is fixed, and can be sensitive to external factors.

Karniel and Inbar (1999) have since explored the use of a simplified model of fractional power damping of the stretch reflex in braking of the ongoing movement. They show that this gives rise to the experimentally observed relationship between movement duration, movement

amplitude, and peak velocity (Hanneton et al., 1997). Although our model (as well as that of Karniel and Inbar) utilizes a pulse-step formulation of the motor command, it is not our intention to posit this formulation as a complete theory of arm movement control. Instead, we wish to demonstrate on a qualitative level that the kinematics of reach can be roughly accounted for by assuming a combination of realistic motor plant dynamics, reflex circuitry, and a simple motor command. Our results call into question theories that make extensive use of highly-detailed motor plans that must be computed prior to reach initiation. In a more complete theory, we imagine allowing a constrained increase in complexity from the pulse-step waveform, as well as on-line adjustment of the motor signals as a function of delayed sensory feedback and motor efference copy. The work of Mussa-Ivaldi (1997) provides one hint as to how to approach the former. In his work, more complex motor signals are achieved by specifying individual pulse-step parameters over a basis set of Gaussian force-fields, which roughly corresponding to the activation of combinations of muscles. The latter issue we have addressed in the context of a simplified controlled system (Barto et al., 1999). We plan to return to these issues with the more realistic arm/muscle/spinal system presented here.

8 Acknowledgments

Preparation of this manuscript was supported by NIH Grant #NIH MH 48185-09 and NSF grant #EIA 9703217. The authors wish to thank Amir Karniel, Zev Rymer, Michael Kositsky, Mark Shapiro, and Richard Nichols for their valuable comments on this manuscript. The authors also thank Leo Zelevinsky and Anders Jonsson for their work on early versions of this model.

9 Appendix

9.1 Muscle Stiffness

We assume that muscle force range in equation 3 is proportional to physiological cross-sectional area (PCSA). We use the PCSA values summarized in (Yamaguchi et al., 1990); the original references are given in table 1. Combining this with equation 3, and assuming that the normalized stiffness (K_n) is equal to 1:

$$K_m = \frac{Q \ PSCA_m}{l_m^r}, \tag{12}$$

where Q is a constant that describes the transformation from physiological cross-sectional area to maximum force, and l_m^r is the length range of muscle m over all feasible skeletal configurations. The l_m^r for each muscle is derived from our model of muscle geometry and given in table 1.

Astryan and Feldman (1965) estimate the joint stiffness of the elbow in a task in which a steady posture was first established against a force at a given joint position (corresponding to $\alpha_6^{(1)}$, $\alpha_6^{(2)}$ and $\alpha_6^{(3)}$ in figure 6B). The force was then suddenly reduced, resulting in a further flexion of the elbow. If we assume that the subjects did not explicitly react to the change in force (as they were instructed), then the joint position at which the elbow came to rest after the force reduction ($\alpha_5^{(*)}$ to to $\alpha_{-45}^{(*)}$) can be interpreted as the point at which the external force is exactly balanced by the tonic stretch reflex for the motor command that was originally established *before* reduction of the external force. Thus, the vertically running curves in figure 6B ($M_{(\psi)}^{(*)}$) can be interpreted as the tonic position-torque response of the muscles as a function of three different motor command magnitudes.

In computing an estimate of tonic stretch reflex gain, we assume that $\alpha_6^{(2)}$ to $\alpha_3^{(2)}$ represents the linear stiffness region for the elbow flexors. A change in load resisted by the elbow of $-.42\ kg{-}m$, or $-4.12N{-}m$, results in a change in elbow position by $8.5°$. We assume that the biceps and brachialis are the two muscle groups primarily involved in resisting the external torque. In our model of muscle geometry, these two muscles reduce their muscle length over this range by 4.5 mm and 4.9 mm, respectively. We also assume that the moment arms are not changing within this region; we therefore arrive at the following relation:

$$\Delta\tau_e \;=\; \Delta F_{brac} R_{e,brac} + \Delta F_{bicep} R_{e,bicep}. \tag{13}$$

Furthermore, if we assume that the moment arms for both muscles are approximately the same (this is a reasonable assumption given our model of muscle geometry: $R_{e,brac} = 3.24\ cm$ and $R_{e,bicep} = 3.47\ cm$), then:

$$\Delta\tau_e \;\approx\; \left(\frac{R_{e,brac} + R_{e,bicep}}{2}\right)(\Delta F_{brac} + \Delta F_{bicep}). \tag{14}$$

Incorporating the linear assumption of stiffness, and equation 12:

$$\Delta\tau_e \;\approx\; \left(\frac{R_{e,brac} + R_{e,bicep}}{2}\right)(\Delta l_{brac}\ K_{brac} + \Delta l_{bicep}\ K_{bicep}); \tag{15}$$

$$\;=\; \left(\frac{R_{e,brac} + R_{e,bicep}}{2}\right)\left(Q\Delta l_{brac}\frac{PCSA_{brac}}{l_{brac}^r} + Q\Delta l_{bicep}\frac{PCSA_{bicep}}{l_{bicep}^r}\right). \tag{16}$$

Finally, solving for Q, we arrive at the following:

$$Q = \frac{2\Delta\tau_e}{R_{e,brac} + R_{e,bicep}} \left(\frac{1}{\frac{\Delta l_{brac} PCSA_{brac}}{l^r_{brac}} + \frac{\Delta l_{bicep} PCSA_{bicep}}{l^r_{bicep}}} \right). \quad (17)$$

In comparing the tonic response of the stretch reflex following either the lengthening or shortening of an active muscle, Gielen and Houk (1984) observed a lower stiffness following a lengthening event. Since we are primarily interested here in the lengthening case, we choose the following estimate of Q to compensate for the shortening condition used by Astryan and Feldman (1965):

$$Q = 0.75 \frac{2\Delta\tau_e}{R_{e,brac} + R_{e,bicep}} \left(\frac{1}{\frac{\Delta l_{brac} PCSA_{brac}}{l^r_{brac}} + \frac{\Delta l_{bicep} PCSA_{bicep}}{l^r_{bicep}}} \right); \quad (18)$$

$$= 202.87. \quad (19)$$

The resulting muscle reflex values are summarized in table 1.

9.2 Extent of muscle exponential region

The extent of the exponential region of each muscle is determined by parameter c in equation 1. We assume that each muscle's c_m is linearly related to the length range of the muscle. Specifically:

$$c_m = C\, l^r_m. \quad (20)$$

We assume that the exponential region of the muscle length-force relationship in (Feldman, 1966) is from $\alpha_0^{(2)}$ (88°) to $\alpha_3^{(2)}$ (111.5°) (See figure 6B). By this, we mean that the exponential term of equation 1 saturates over this range. Thus:

$$c_m \approx (1 - e^{-1}) \Delta\hat{l}_m, \quad (21)$$

where $\Delta\hat{l}_m$ is the change of muscle length over the exponential region. For the elbow flexors, $\Delta\hat{l}_{brac} = 2.52\ cm$ and $\Delta\hat{l}_{bicep} = 2.62\ cm$.

Utilizing the average length change and length range of the brachialis and biceps, we estimate C as follows:

$$C \approx \left(1 - e^{-1}\right) \frac{\Delta \hat{l}_{brac} + \Delta \hat{l}_{bicep}}{l^r_{brac} + l^r_{bicep}}; \tag{22}$$

$$= 10.23\ . \tag{23}$$

Thus, c_{brac} =0.91 cm and c_{bicep} =2.34 cm. The remaining parameters are given in table 1.

9.3 Stiffness of flexor carpi radialis

An et al. (1981) report the PCSA of flexor carpi radialis as 2.0 cm^2. Given equation 12, we arrive at $K_{fcr} = 8610\ N/m$.

References

Amis, A. A., Dowson, D., and Wright, V. (1979). Muscle strengths and musculo-skeletal geometry of the upper limb. *Engineering in Medicine*, 8(1):41–48.

An, K. N., Hui, F. C., Morrey, B. F., Linscheid, R. L., and Chao, E. Y. (1981). Muscles across the elbow joint: A biomechanical analysis. *Journal of Biomechanics*, 14(10):659–669.

Astryan, D. G. and Feldman, A. G. (1965). Functional tuning of nervous system with control of movement or maintenance of a steady posture – i. mechanographic analysis of the work of the joint on execution of a postural task. *Biophysics USSR*, 10:925–935.

Barto, A. G., Fagg, A. H., Sitkoff, N., and Houk, J. C. (1999). A cerebellar model of timing and prediction in the control of reaching. *Neural Computation*, 11:565–594.

Binder, M. D., Heckman, C. J., and Powers, R. K. (1996). The physiological control of motorneuron activity. In Rowell, L. B. and Shepherd, J. T., editors, *Handbook of Physiology*, chapter 1. Oxford University Press, New York.

Bizzi, E., Chapple, W., and Hogan, N. (1982). Mechanical properties of muscles: Implications for motor control. *Trends in Neuroscience*, 5:395–398.

Bizzi, E., Hogan, N., Mussa-Ivaldi, F. A., and Giszter, S. (1992). Does the nervous system use equilibrium-point control to guide single and multiple joint movements? *Behavioral and Brain Sciences*, 15:603–613.

Chang, S. L., Wu, C. H., and Lee, D. T. (1999). A muscular-like compliance control for active vehicle suspension. In *Proceedings of the 1999 IEEE International Conference on Robotics and Automation*, pages 3275–3280.

Engelbrecht, S. E. (1999). Minimum principles in motor control. *Journal of Mathematical Psychology, in press.*

Fagg, A. H. (2000). A model of muscle geometry for a two degree-of-freedom planar arm. Technical Report 00-03, Department of Computer Science, University of Massachusetts, Amherst.
http://www-anw.cs.umass.edu/papers/2000/muscle.html.

Feldman, A. G. (1966). Functional tuning of the nervous system with control of movement or maintenance of a steady posture. II Controllable parameters of the muscle. *Biophysics*, 11:565–578.

Feldman, A. G., Adamovich, S. V., Ostry, D. J., and Flanagan, J. R. (1990). The origin of electromyograms - Explanations based on the equilibrium point hypothesis. In Winters, J. M. and Woo, S. L.-Y., editors, *Multiple Muscle Systems: Biomechanics and Movement Organization*, pages 195–213. Springer-Verlag, New York.

Flanagan, J. R., Ostry, D. J., and Feldman, A. G. (1993). Control of trajectory modifications in target-directed reaching. *Journal of Motor Behavior*, 25:140–152.

Freivalds, A. (1985). Incorporation of active elements into the articulated total body model. Technical Report AAMRL-TR-85-061, Armstrong Aerospace Medical Research Laboratory, Wright-Patterson Air Force Base.

Georgopoulos, A. P. and Grillner, S. (1989). Visuomotor coordination in reaching and locomotion. *Science*, 245:1209–1210.

Ghez, C. (1979). Contributions of central programs to rapid limb movement in the cat. In Asanuma, H. and Wilson, V. J., editors, *Integration in the Nervous System*, pages 305–320. Igaku-Shoin, Tokyo.

Ghez, C. and Martin, J. H. (1982). The control of rapid limb movement in the cat. III. Agonist-antagonist coupling. *Experimental Brain Research*, 45:115–125.

Gielen, C. C. A. M. and Houk, J. C. (1984). Nonlinear viscosity of human wrist. *Journal of Neurophysiology*, 52:553–569.

Gielen, C. C. A. M. and Houk, J. C. (1986). Simple changes in reflex threshold cannot explain all aspects of rapid voluntary movements. *Behavior & Brain Science*, pages 605–607.

Gielen, C. C. A. M. and Houk, J. C. (1987). A model of the motor servo: Incorporating nonlinear spindle receptor and muscle mechanical properties. *Biological Cybernetics*, 57:217–231.

Gottlieb, G. L. (1996). On the voluntary movement of compliant (inertial-viscoelastic) loads by parcellated control mechanisms. *Journal of Neurophysiology*, 76(5):3207–3229.

Gribble, P. L., Ostry, D. J., Sanguineti, V., and Laboissière, R. (1998). Are arm control signals required for human arm movement? *Journal of Neurophysiology*, 79(3):1409–1424.

Hannaford, B. and Stark, L. (1985). Roles of the elements of the triphasic control signal. *Experimental Neurology*, 90:619–634.

Hanneton, S., Berthoz, A., Droulez, J., and Slotine, J. J. E. (1997). Does the brain use sliding variables for the control of movements? *Biological Cybernetics*, 73:381–393.

Hasan, Z. (1983). A model of spindle afferent response to muscle stretch. *Journal of Neurophysiology*, 49(4):989–1006.

Hasan, Z. and Houk, J. C. (1975). Transition in sensitivity of spindle receptors that occurs when muscle is stretched more than a fraction of a millimeter. *Journal of Neurophysiology*, 38:673–689.

Hill, A. V. (1938). The heat of shortening and the dynamic constants of muscle. *Proc. Roy. Soc. (London), ser. B*, 126:136–195.

Hogan, N. (1984). Adaptive control of mechanical impedance by coactivation of antagonist muscles. *IEEE Transactions on Automatic Control*, AC-29:681–690.

Hogan, N., Bizzi, E., Mussa-Ivaldi, F., and Flash, T. (1987). Controlling multijoint motor behavior. *Exercise and Sports Review*, pages 153–190.

Hollerbach, J. and Flash, T. (1982). Dynamic interactions between limb segments during planar arm movement. *Biological Cybernetics*, 44:67–77.

Houk, J. C. (1981). Afferent mechanisms mediating autogenetic reflexes. In Pompeiano, O. and Marsan, C. A., editors, *Brain mechanisms of perceptual awareness*, pages 167–181. Raven.

Houk, J. C., Crago, P. E., and Rymer, W. Z. (1981). Function of the spindle dynamic response in stiffness regulation–a predictive mechanism provided by non-linear feedback. In Taylor, H. and Prochazka, A., editors, *Muscle Receptors and Movement*, pages 299–309. Macmillan, London.

Houk, J. C. and Rymer, W. Z. (1981). Neural control of muscle length and tension. In Brooks, V. B., editor, *Handbook of Physiology: Sec. 1: Vol. 2. Motor Control*, pages 247–323. American Physiological Society, Bethesda, MD.

Houk, J. C., Rymer, W. Z., and Crago, R. E. (1992). Responses of muscle spindle receptors to transitions in stretch velocity. In Jami, L., Pierrot-Deseilligny, E., and Zytnicki, D., editors, *Muscle Afferents and Spinal Control of Movement*, pages 53–61. Pergamon, NY. IBRO Symposium, 16–19 September 1991 at the College de France, Paris, France.

Houk, J. C., Singer, J. J., and Goldman, M. R. (1970). An evaluation of length and force feedback to soleus muscles of decerebrate cats. *Journal of Neurophysiology*, 33:784–811.

Jordan, M. I., Flash, T., and Arnon, Y. (1994). A model of the learning of arm trajectories from spatial deviations. *Journal of Cognitive Neuroscience*, 6:359–376.

Karniel, A. and Inbar, G. F. (1997). A model of learning human reaching movements. *Biological Cybernetics*, 77:173–183.

Karniel, A. and Inbar, G. F. (1999). The use of a nonlinear muscle model in explaining the relationship between duration, amplitude, and peak velocity. *Journal of Motor Behavior*, 31(3):203–206.

Katayama, M. and Kawato, M. (1993). Virtual trajectory and stiffness ellipse during multi-joint arm movement predicted by neural inverse models. *Biological Cybernetics*, 69:353–362.

Keller, E. L. and Robinson, D. A. (1971). Absence of stretch reflex in extraocular muscles of the monkey. *Journal of Neurophysiology*, 34:908–919.

Lestienne, F. (1979). Effects of inertial load and velocity on the braking process of voluntary limb movements. *Experimental Brain Research*, 35:407–418.

Lin, D. C. and Rymer, W. Z. (1998). Damping in reflexively active and areflexive lengthening muscle evaluated with inertial loads. *Journal of Neurophysiology*, 80(6):3369–3372.

Lukashin, A. V., Amirikian, B. R., and Georgopoulos, A. P. (1996). Neural computations underlying the exertion of force A model. *bc*, 74:469–478.

Massone, L. L. E. and Myers, J. D. (1996). The role of plant properties in arm trajectory formation: A neural network study. *IEEE Transactions on Systems, Man, and Cybernetics*, 26:719–732.

Miller, L. E. and Sinkjaer, T. (1998). Primate red nucleus discharge encodes the dynamics of limb muscle activity. *Journal of Neurophysiology*, 80:59–70.

Mussa-Ivaldi, F. A. (1992). From basis functions to basis fields: Vector field approximation from sparse data. *Biological Cybernetics*, 67:479–489.

Mussa-Ivaldi, F. A. (1997). Nonlinear force fields: A distributed system of control primitives for representing and learning movements. In *Proceedings of the IEEE International Symposium on Computational Intelligence in Robotics and Automation–CIRA 1997*, pages 84–90. IEEE Computer Society Press.

Nichols, T. R. and Houk, J. C. (1976). Improvement in linearity and regulation of stiffness that results from actions of stretch reflex. *Journal of Neurophysiology*, 39(1):119–142.

Partridge, L. D. (1979). Muscle properties: A problem for the motor controller physiologist. In Talbott, R. E. and Humphries, D. R., editors, *Posture and Movement*, pages 189–229. Raven Press, NY.

Peterson, B., Baker, J. F., Iwamoto, Y., Perlmutter, S. I., and Quinn, K. (1992). Neuronal substrates of vestibular reflex control of eye and head movements. In Shimazu, H. and Shinoda, Y., editors, *Vestibular and Brain Stem Control of Eye, Head and Body Movements*, pages 53–68. Japan Scientific Societies Press, Tokyo, Japan.

Ramos, C., Stark, L., and Hannaford, B. (1989). Time optimality, proprioception, and the triphasic emg pattern. *Behavioral and Brain Sciences*, 12:231–232.

Ramos, C. F. and Stark, L. W. (1987). Simulation studies of descending and reflex control of fast movements. *Journal of Motor Behavior*, 19(1):38–61.

Robinson, D. A. (1975). Oculomotor control signals. In Lennerstrand, G. and Bach-y-rita, P., editors, *Basic Mechanisms of Ocular Motility and their Clinical Implications*, pages 337–374. Pergamon Press, Oxford.

van Dijk, J. H. M. (1978). Simulation of human arm movements controlled by peripheral feedback. *Biological Cybernetics*, 29:175–186.

van Sonderen, J. F. and Denier van der Gon, J. J. (1990). A simulation study of a programme generator for centrally programmed fast two-joint arm movements: Responses to single- and double-step target displacements. *Biological Cybernetics*, 63:35–44.

Winters, J. M. (1990). Hill-based muscle models: A systems engineering perspective. In Winters, J. M. and Woo, S. L.-Y., editors, *Multiple Muscle Systems: Biomechanics and Movement Organization*, pages 69–93. Springer-Verlag, New York.

Winters, J. M. and Stark, L. (1987). Muscle models: What is gained and what is lost by varying model complexity. *Biological Cybernetics*, 55:403–420.

Winters, J. M. and Stark, L. (1988). Estimated mechanical properties of synergistic muscles involved in movements of a variety of human joints. *Journal of Biomechanics*, 21:1027–1041.

Wu, C. H., Houk, J. C., Young, K. Y., and Miller, L. E. (1990). Nonlinear damping of limb motion. In Winters, J. M. and Woo, S. L.-Y., editors, *Multiple Muscle Systems: Biomechanics and Movement Organization*, pages 214–235. Springer–Verlag, New York.

Wu, C. H., Hwang, K. S., and Chang, S. L. (1997). Analysis and implmentation of a neuromuscular-like control for robotic compliance. *IEEE Transactions on Control Systems Technology*, 5(6):586–597.

Yamaguchi, G. T., Sawa, A. G., Moran, D. W., Fessler, M. J., and Winters, J. M. (1990). A survey of human musculotendon actuator parameters. In Winters, J. M. and Woo, S. L.-Y., editors, *Multiple Muscle Systems: Biomechanics and Movement Organization*, pages 717–773. Springer-Verlag, New York.

Contents